NANOSYSTEMS:
PHYSICS, CHEMISTRY, MATHEMATICS

Kameneva S.V., et al. *Nanosystems: Phys. Chem. Math.*, 2022, **13** (4), 404–413.
http://nanojournal.ifmo.ru
DOI 10.17586/2220-8054-2022-13-4-404-413

Original article

Photochromic aerogels based on cellulose and chitosan modified with WO_3 nanoparticles

Svetlana V. Kameneva[1,a], Matvei A. Popkov[1,2,b], Ilya V. Tronev[1,3,c], Sergey Yu. Kottsov[1,2,d], Madina M. Sozarukova[1,e], Vladimir K. Ivanov[1,f]

[1]Kurnakov Institute of General and Inorganic Chemistry of the Russian Academy of Sciences, Moscow, Russia
[2]Lomonosov Moscow State University, Moscow, Russia
[3]HSE University, Moscow, Russia

[a]kamenevasvetlanav@gmail.com, [b]popkovma2001@mail.ru, [c]ivtronev@edu.hse.ru,
[d]sergey12-17@yandex.ru, [e]s_madinam@bk.ru, [f]van@igic.ras.ru

Corresponding author: S. V. Kameneva, kamenevasvetlanav@gmail.com

PACS 68.65.k, 81.20.n

ABSTRACT In this work, we report the first synthesis of photochromic aerogels and films based on TEMPO-oxidized cellulose and chitosan modified with tungsten trioxide nanoparticles. The blue coloring of aerogels based on WO_3-modified biopolymers under UV light occurs due to the reduction of W^{+6} to W^{+5}. The coloration of films of the same composition occurs due to the reduction of W^{+6} to W^{+5} and W^{+4}. The photochromic properties of aerogels and films are reversible; oxidation by atmospheric oxygen leads to bleaching of materials. At that, films become colorless within a few days while aerogels with a high specific surface area (200 m^2/g) become colorless within several minutes. The antioxidant properties of the WO_3 sol and the WO_3/TEMPO-oxidized cellulose/chitosan composite were studied by luminol-activated chemiluminescence method. The antioxidant capacity of WO_3/TEMPO-oxidized cellulose/chitosan gel is 1.5 times higher than that of the commercially available antioxidant mexidol.

KEYWORDS Aerogel, hybrid materials, nanocomposite, biopolymers, cellulose, chitosan, tungsten oxide, photochromic material, antioxidant.

ACKNOWLEDGEMENTS S.V. Kameneva thanks the Council for Grants of the President of the Russian Federation for supporting the study (SP-4398.2021.4).

FOR CITATION Kameneva S.V., Popkov M.A., Tronev I.V., Kottsov S.Yu., Sozarukova M.M., Ivanov V.K. Photochromic aerogels based on cellulose and chitosan modified with WO_3 nanoparticles. *Nanosystems: Phys. Chem. Math.*, 2022, **13** (4), 404–413.

1. Introduction

Cellulose and chitosan are biopolymers that easily undergo chemical modifications, including the introduction of functional groups and cross-linking with other polymers [1–4]. These biopolymers form aqueous dispersions, flexible films, gels and aerogels, effectively adsorb metal cations and inorganic nanoparticles due to the formation of hydrogen and coordination bonds [5, 6]. These qualities make cellulose and chitosan convenient matrices for creating hybrid materials modified with inorganic nanoparticles. Aerogels based on chemically modified cellulose have great potential for application in medicine as moisture-absorbing dressings, biocompatible scaffolds for tissue engineering, in drug delivery systems and can also act as carriers of catalysts, adsorbents, etc. [1, 7–12]. Recently, a work devoted to the creation of a photochromic aerogel based on cellulose modified with an avobenzone derivative was published [13].

Nanosized tungsten trioxide is a semiconductor material with unique photochromic, electrochromic and photocatalytic properties. WO_3 effectively absorbs UV and visible radiation, while the material turns blue due to the reduction of W^{+6} to W^{+5} and W^{+4}. Oxidation of W^{+4} and W^{+5} and bleaching of the material can occur by the atmospheric oxygen. The coordination of some organic ligands containing hydroxyl or amino groups to the surface of WO_3 nanoparticles can increase the rate of the photochromic reaction, increase the color intensity and allow one to repeat the coloration–discoloration cycle [14–16]. Coloration of WO_3 can also occur in a reducing atmosphere which its application as a gas sensor is based on [17–19].

Practically significant property of tungsten trioxide is its antibacterial activity. WO_3/hydroxyethylcellulose membranes have been shown to promote wound healing, possess an anti-inflammatory effect and also demonstrate antibacterial activity against both Gram-positive and Gram-negative bacteria [20]. Under the action of UV radiation, the antibacterial properties of tungsten trioxide stabilized with polyvinylpyrrolidone are significantly enhanced due to its photocatalytic effect, which leads to the destruction of the bacterial cell wall n [21]. WO_3 nanoparticles are toxic in some cases and for

their biomedical applications polymer coatings are used. For example, the toxicity of WO_3 to human cells (human dermal fibroblast cell line) was successfully reduced by its immobilization in a hydroxyethyl cellulose matrix n [20]. Prospects for the biomedical application of nanomaterials based on tungsten trioxide actualize the problem of analyzing their redox activity in relation to various species involved in free radical homeostasis n [22–24], including hydrogen peroxide, being one of the important reactive oxygen species (ROS) n [25, 26].

Up to date the investigations of photochromic properties of hybrid materials based on cellulose modified with WO_3 nanoparticles have been reported only in a few works [14, 15, 27]. In this study, we propose for the first time a synthetic procedure which allows one to obtain aerogels based on TEMPO-oxidized cellulose and chitosan modified with WO_3 nanoparticles. The morphological, hydrophilic, photochromic and antioxidant properties of such aerogels have been studied. The resulting aerogels appear to be promising materials for the development of absorbent wound dressings with antibacterial and antioxidant effects, as well as for the design of UV radiation visualizers and gas sensors.

2. Materials and methods

2.1. Reagents

The following reagents were used in the study: sodium tungstate $Na_2WO_4{\cdot}2H_2O$ (Rushim), TEMPO 2,2,6,6-tetramethylpiperidine-1-oxyl (99%, NIOC SB RAS), sodium hypochlorite NaClO 19% (PCG), sodium bromide NaBr (Lavernalab), filtering paper (blue ribbon), hydrochloric acid HCl 36% (Chimmed), sodium hydroxide NaOH (Chimmed), cation exchange resin, hydrogen peroxide 30% (Chimmed), luminol 97% (Aldrich), potassium dihydrogen phosphate (for cell cultures, Aldrich), polyvinylpyrrolidone (10000, Aldrich), mexidol (6-methyl-2-ethyl-3-hydroxypyridine succinate, Pharmasoft).

2.2. Synthesis of WO_3 nanoparticles

200 ml of cation exchange resin in a protonated form was placed in a separating funnel. A 0.005 M solution of Na_2WO_4 was slowly added to the funnel, maintaining the rate of outflow of the solution from the funnel within 1–2 drops per second. At the outlet of the funnel, a solution of unstable tungstic acid ($WO_2{\cdot}H_2O$) with a pH of about 3 was collected. 1.33 g of PVP was added to 50 ml of the resulting solution and heated to 90°C for two hours with stirring. The WO_3 sol concentration was determined gravimetrically.

2.3. TEMPO-oxidation of cellulose

4.00 g of finely cut filter paper (blue ribbon) was placed in 250 ml of 5 M HCl solution and stirred at 80°C for 40 minutes. The resulting cellulose dispersion was then poured into 1.5 L of cold distilled water to stop the hydrolysis. The resulting nanocrystalline cellulose was washed with distilled water until pH 6. The resulting mixture was kept for 40 minutes in an ultrasonic bath at a temperature not exceeding 18°C to obtain a homogeneous dispersion. The concentration of nanocrystalline cellulose in the dispersion was about 3%.

Weighed portions of TEMPO (0.064 g) and NaBr (0.400 g) were placed in a 1 L beaker, 200 ml of distilled water was added and the mixture was stirred until complete dissolution. The nanocrystalline cellulose dispersion was then added and stirred for additional 10 minutes, followed by addition of 25 ml of 11.9% NaClO with constant stirring. Oxidation reaction was carried out with regular dropwise addition of 0.3 M NaOH from a burette, maintaining pH within 10.5–11 range. After the pH remained constant for 30 minutes, 0.5 M HCl was added to pH 6.5–7 and the mixture was stirred for 15 minutes. The resulting pulp was washed with distilled water and centrifuged. Then ultrasonic dispersion was carried out for 40 min at 15–20°C. The concentration of TEMPO-oxidized cellulose was determined gravimetrically.

The yield of the oxidation reaction was found by conductometric titration. The concentration of carboxyl groups was 600–800 mmol per g of cellulose, the degree of carboxylation was about 10%.

2.4. Synthesis of hybrid aerogels and films

A solution of chitosan was added to the TEMPO-oxidized cellulose dispersion, while stirring in an ultrasonic bath. Then a solution of $WO_3{\cdot}H_2O$ was added dropwise until a homogeneous mixture was formed. To obtain the films, the resulting dispersion was placed in Petri dishes and dried at room temperature. The concentrations were chosen so that the molar ratio of the formula units of tungsten oxide (WO_3), chitosan ($C_6H_{11}O_5N$) and cellulose ($C_6H_{12}O_6$) in the composite (W–CC) was 1/2/8.

To obtain aerogels, the dispersion was left for 7 days for the formation of hydrogels and aging. The obtained hydrogels were placed in isopropanol to replace the solvent, isopropanol was changed daily for 5 days.

Similarly, composites of chitosan and TEMPO-oxidized cellulose without tungsten oxide (CC) were obtained.

The sample was dried in an installation consisting of a Supercritical 24 high-pressure pump (SSI, USA), a 50-mL steel reactor and a back pressure regulator BPR (Go Regulator, Waters, USA). The sample was washed for 3 h with supercritical CO_2 at 50°C and 148 atm. Then, within 30–40 minutes the pressure in the heated autoclave was gradually reduced to atmospheric pressure. As a result, monolithic aerogels were obtained.

2.5. Characterization methods

Scanning electron microscopy (SEM) images were obtained on a Carl Zeiss NVision 40 electron microscope at an accelerating voltage of 3 kV; the samples were preliminarily deposited with a carbon coating. Elemental analysis and element distribution maps were obtained using an X-Max Oxford Instruments detector (UK) at an accelerating voltage of 20 kV with a cobalt standard.

X-ray diffraction data (XRD) was measured on a Bruker D8 Advance diffractometer using CuKa radiation in the 2θ range from 5° to 80°.

Vibrational spectra were recorded on an INFRALUM FT-08 FTIR spectrometer in the range from 400 to 4000 cm^{-1} with a 4 cm^{-1} resolution.

UV visible reflectance spectra and coloration kinetics of composites were obtained on an Ocean Optics QE65000 spectrometer in the range of 250–1000 nm with a resolution of 1 nm using an HPX-2000 xenon lamp.

The hydrodynamic radius and ζ-potential were measured using a Photocor Compact Z analyzer with a thermally stabilized 638 nm semiconductor laser.

The specific surface area of films and aerogels (S_{BET}) was measured by low-temperature nitrogen adsorption on an ATX-06 analyzer (Katakon, Russia). Before the analysis, samples were degassed for 2 hours at 80°C in vacuum. The specific surface area for the samples was calculated by the Brunauer-Emmett-Teller (BET) method in the range of nitrogen partial pressures of 0.05–0.25. The calculation of the pore size distribution was calculated from the nitrogen desorption isotherm by the Barrett-Joyner-Halend (BJM) method in the range of nitrogen partial pressures of 0.05–0.97.

The antioxidant properties of the samples were analyzed by luminol-activated chemiluminescence using a 12-channel "Lum-1200" chemiluminometer (DISoft). The ROS generating system contained hydrogen peroxide and luminol was used as a chemiluminescent probe. The technique of chemiluminescence analysis is described in detail in [28]. The required amounts of luminol (50 μM) and H_2O_2 (980 μM) were added to cuvettes with phosphate buffer solution (100 mM, pH 7.4), the total volume of the system was 1.000 ml. The signal was recorded at 37°C. After reaching the maximum intensity of chemiluminescence, aliquots of the studied samples were added to the cuvettes. Simultaneously the luminescence was recorded for the control sample and samples with different concentrations of the studied compositions (W–CC with WO_3 concentrations from 50 to 1000 μM; WO_3 with concentrations from 50 to 300 μM; the commercially available antioxidant mexidol with concentrations from 30 to 110 μM). The integral intensity was chosen as an analytical signal, i.e., the area under the chemiluminescent curve for a selected time interval, which is proportional to concentration of free radicals.

3. Results and discussion

3.1. Formation of the gels

Biopolymer-based composite gels were obtained by gradually adding a solution of chitosan to the aqueous dispersion of cellulose. Since the viscosity of chitosan solution is sufficiently high, the chitosan drops slowly dissolved in the volume of the cellulose dispersion. An immediate gel formation was observed at the boundary of chitosan droplets with dispersion. To obtain a homogeneous material, a mixture of chitosan and cellulose was homogenized in an ultrasonic bath for 10 minutes under vigorous stirring. Then, a sol of WO_3 nanoparticles was added to the gel and redispersed in an ultrasonic bath.

Immediately after homogenization the gels did not retain their shape and deformed under the action of gravity. For further gelation and aging, they were transferred into plastic containers and stored in the dark for 5–7 days at room temperature.

The formation of biopolymer gels at the first stage occurs due to ionic interactions between cellulose and chitosan. TEMPO-oxidized cellulose is a polyanion due to partial dissociation of carboxyl groups; the ζ-potential of nanocrystalline cellulose particles obtained in this work is -30 mV. The amino groups of chitosan are partially protonated in the presence of hydrochloric acid, which leads to the formation of a polycationic biopolymer. It is noteworthy that WO_3 nanoparticles with negative ζ-potential of about -20 mV are reliably immobilized on polycationic chitosan molecules.

Apparently, the interaction of cationic groups of cellulose and anionic groups of chitosan is not strong enough to produce a gel that retains its shape. During gel aging, new hydrogen bonds between O–H groups of biopolymers are gradually formed which leads to the formation of a stronger network. As a result, after several days of aging the gel ceases to deform under the action of gravity when the container is tilted.

Drying freshly prepared WO_3–CC and CC gels at room temperature and atmospheric pressure results in the formation of transparent flexible films.

After aging, the WO_3–CC and CC gels were subjected to a solvent change to isopropanol and then dried in supercritical CO_2 at a pressure of 150 atm and a temperature of 50°C. As a result, monolithic opaque aerogels were obtained (Fig. 1). At the same time, no shrinkage of the materials occurred during the solvent replacement and drying.

3.2. Characterization of hybrid materials

The CC and W–CC films are composed of rod-shaped cellulose nanoparticles tightly adjacent to each other (Fig. 1A). The porous structure of CC and WO_3–CC aerogels is formed by a disordered network of cellulose nanoparticles (Fig. 1B). According to previously published data [27], the size of WO_3 nanoparticles obtained by ion exchange from sodium tungstate is about 2 nm. Prepared WO_3 nanoparticles cannot be studied by SEM. However, the EDX analysis confirmed the uniform distribution of tungsten in both the W–CC film and the W–CC aerogel (Fig. 1C,D). The specific surface area of CC and W–CC aerogels is about 200 m^2/g. The W–CC hybrid aerogel contains both mesopores with a diameter of 5 and 10–30 nm and macropores (Fig. 2). The geometric density of aerogels CC and W–CC is about 0.04 g/cm^3.

During the development of materials for biomedical applications, it is important to study the ability of the material to absorb water. In this work, to study the absorption capacity, samples of materials of known weight were immersed in distilled water for 30 minutes, after which the weight of the samples with absorbed water was measured. Films obtained by drying a chitosan solution at room temperature completely dissolve in water within a few minutes. In turn, TEMPO-oxidized cellulose films remain intact and practically do not swell, absorbing about 2 g of water per 1 g of film. Composite films of TEMPO-oxidized cellulose and chitosan (CC) and W–CC hybrid films swell in water, absorbing about 8 g of water per 1 g of material. In this case, the films increase in volume but retain their integrity. Swelling occurs due to hydration of chitosan molecules while integrity is maintained due to electrostatic binding of polycationic chitosan molecules with polyanionic cellulose molecules. Aerogels CC and W–CC absorb about 20 g of water per 1 g of material. The volume of aerogels does not change after absorbing water because the water molecules fill the existing pores in the material.

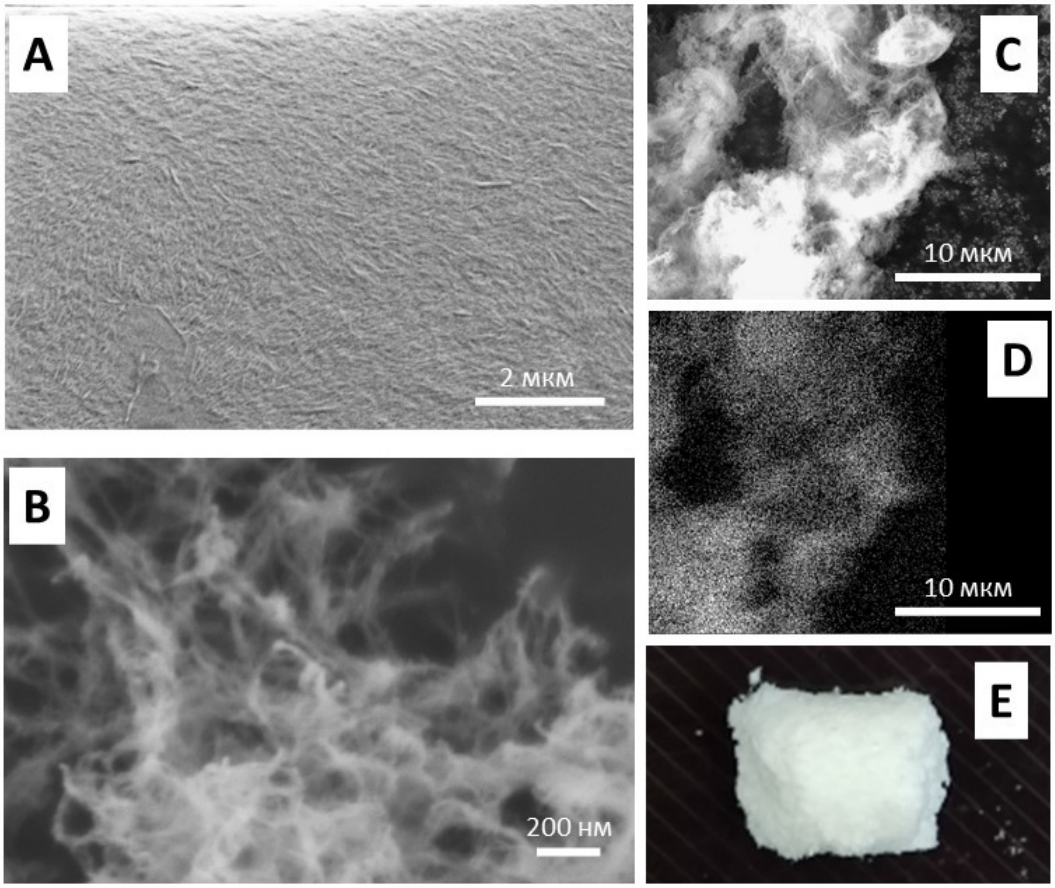

FIG. 1. SEM images of W–CC film (A) and W–CC aerogel (B) at an accelerating voltage of 3 kV; micrograph of W–CC aerogel (C) and distribution of W (D) according to EDX data at an accelerating voltage of 20 kV; the image of W–CC aerogel (E)

The IR spectra of the CC and W–CC composites contain absorption bands which belong to cellulose and chitosan molecules (Fig. 3A). The absorption bands of O–H stretching vibrations of cellulose and chitosan overlap with the absorption band of N–H stretching vibrations of chitosan, forming a wide band in the region of 3100–3500 cm^{-1}. Bands corresponding to stretching and bending vibrations of C–H are observed in the regions of 2900 cm^{-1} and 1200–1500 cm^{-1}, respectively. The absorption bands in the region of 900–1200 cm^{-1} refer to skeletal vibrations of biopolymers. The absorption bands in the region of 1550–1700 cm^{-1} refer to the bending vibrations of O-H in the molecules of both biopolymers and the NH_2 group of chitosan. The shoulder at 1730 cm^{-1} refers to the vibrations of the carboxyl group of

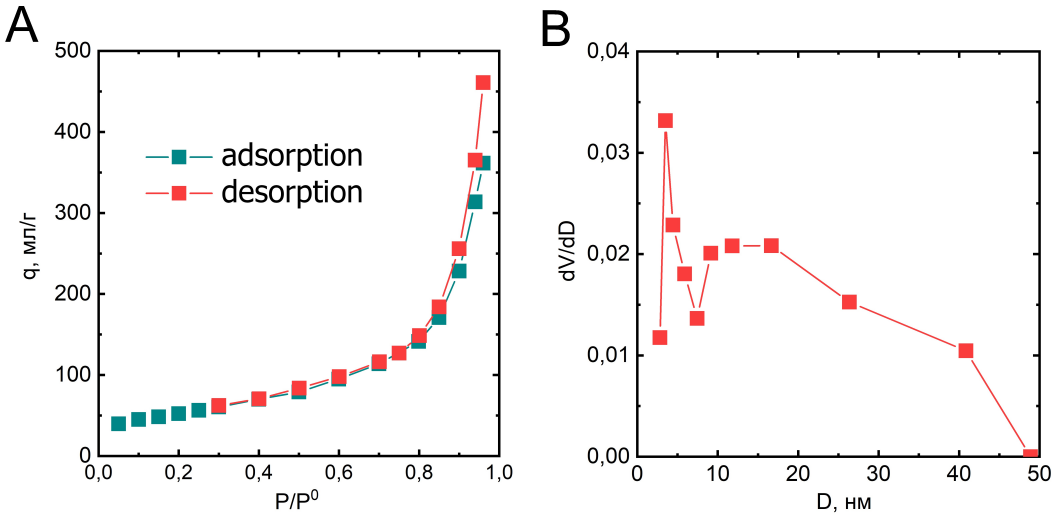

FIG. 2. Nitrogen adsorption and desorption isotherms (A) for W–CC aerogel and pore size distribution (B)

TEMPO-oxidized cellulose. In addition to the absorption bands of cellulose and chitosan, the W–CC spectrum contains absorption bands of W=O and O–W–O at 963 and 805 cm^{-1}, respectively (Fig. 3B).

Particles of TEMPO-oxidized cellulose contain crystalline regions with the Iβ structural type, which follows from the appearance of peaks at angles of 16° (110) and 23° (200) in the XRD patterns of the composites (Fig. 3C). The size of the crystalline regions is about 3 nm, as estimated from the Scherrer formula. Nanoparticles of WO_3 have an amorphous structure; in XRD of the W–CC composite the tungsten oxide corresponds to a wide halo at small angles.

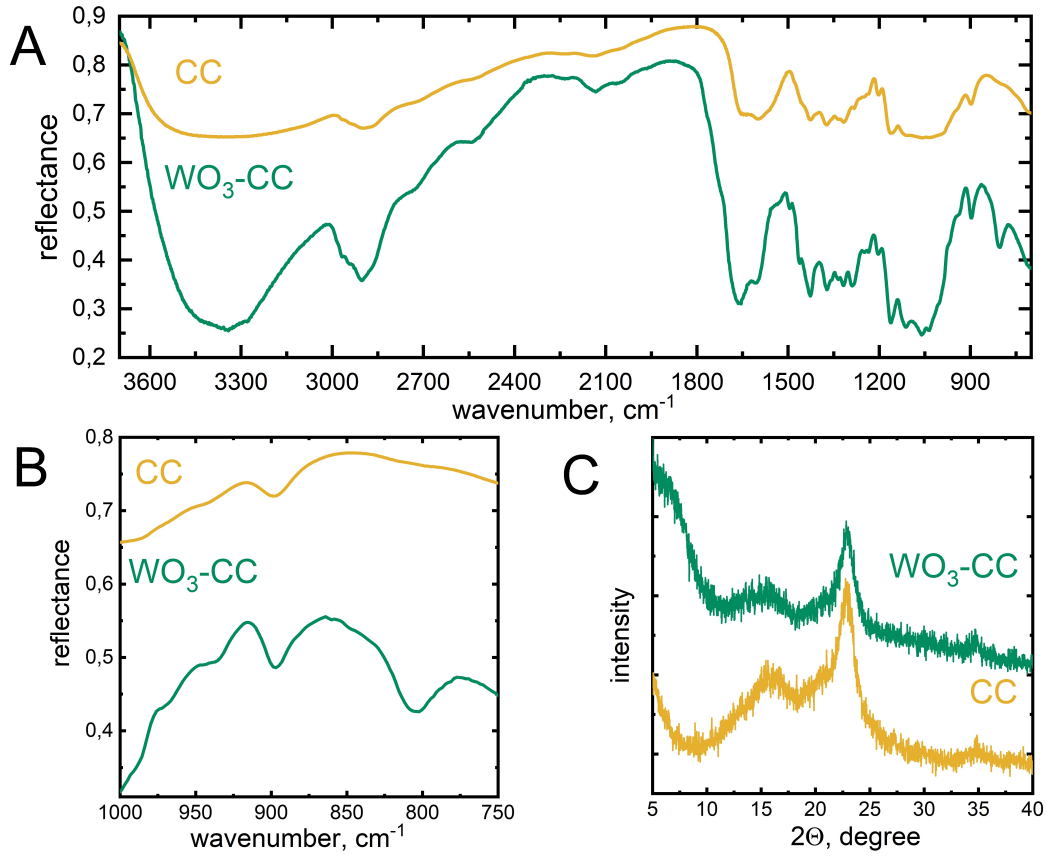

FIG. 3. IR spectra of W–CC and CC aerogels (A and B); XRD pattern of W–CC and CC aerogels (C)

3.3. Photochromic properties

The absorption edge in the UV region of hybrid films and aerogels is located at about 390 nm. The band gap of semiconducting WO_3 nanoparticles in aerogels and W–CC films determined from the data of UV-Vis spectroscopy is about 3.2 eV. Both films and aerogels containing WO_3 exhibited reversible photochromic properties. Under the action of UV radiation, the films were colored in an intense blue color and aerogels were colored in light blue. The absorption of radiation with an energy exceeding the band gap initiates the transition of electrons to the conduction band of the semiconductor oxide and then the delocalized electron is able to reduce metal ions [15]. The mechanism of photochromic reactions is associated with the reduction of W^{+6} in nanodispersed tungsten oxide to lower oxidation states – W^{+5} and W^{+4}. The UV-Vis spectra of blue films and W–CC aerogels (Fig. 4A) contain absorption bands in the visible region related to W^{+5} (770 nm) and W^{+4} (630 nm) ions [29]. The coloration kinetics of films and aerogels were studied using a xenon lamp as a source of both UV radiation initiating photochromic reaction and probing irradiation of the spectrometer. During the irradiation of W–CC aerogels the intensity of the absorption band at 770 nm increases rapidly, the absorption band at 630 nm appears with an induction period of about 2 minutes (Fig. 4B). Thus, successive reduction processes $W^{+6} \rightarrow W^{+5} \rightarrow W^{+4}$ occur in the aerogel under the action of UV radiation. When the W–CC film is irradiated, at the initial stage the absorption bands at 770 and 630 nm simultaneously grow (Fig. 4B). After 3 minutes the growth rate of the 700 nm band intensity decreases, while the intensity of the band at 630 nm continues to increase almost linearly. Evidently, the reduction rate $W^{+5} \rightarrow W^{+4}$ in the film is higher than in the aerogel.

The in-dark bleaching of UV-irradiated aerogels and films is associated with the oxidation of tungsten ions by atmospheric oxygen. The discoloration kinetics of the materials was measured using a halogen lamp as the spectrometer light source to minimize the effects of UV radiation on the samples. The rate of discoloration for aerogels is much higher than for the films (Fig. 4C). The aerogels became colorless within minutes, while the films became colorless after 5 days. The higher bleaching rate of the W–CC aerogel in comparison with the film is associated with higher availability of the reaction centers of WO_3 nanoparticles to oxygen molecules, since the surface area of the aerogel is several orders of magnitude higher than the surface area of the film.

3.4. Antioxidant properties

Hydrogen peroxide and free radicals formed during its decomposition are presented in significant amounts among metabolites in the process of wound healing [30]. Despite the important role of hydrogen peroxide as a cytotoxic component, at present, special attention is paid to its functioning as a signaling molecule, as well as its participation in the regulation of transcription factors [31–33].

If the metabolism is disturbed in damaged tissues an excess of free radicals occurs, which provokes oxidative stress and prevents wound healing. In this case, treatment should include the use of antioxidants – substances that irreversibly react with free radicals. Another way to deal with the oxidative stress is to use enzymes that catalyze the decomposition of hydrogen peroxide into oxygen and water (for example, catalase). The disadvantage of this approach is the high cost of enzyme preparations manufacture. It has been shown recently that inorganic nanomaterials, for example, nanoparticles of cerium dioxide [34] and hematite (α-Fe_2O_3) [35] can exhibit catalase-like activity [36]. The synthesis and investigation of new inorganic analogues of enzymes, nanozymes can contribute to the problem of fighting the oxidative stress during treatment of various diseases.

The antioxidant properties of the W–CC composite were studied by luminol-activated chemiluminescence. The experiment was carried out under conditions close to physiological (37°C, pH 7.4). The molecular ROS generating system consisted of hydrogen peroxide and a luminol chemiluminescent probe. The oxidation of luminol upon interaction with radicals is accompanied by luminescence, the intensity of which is recorded by a chemiluminometer. In the presence of compounds with antioxidant properties the luminescence intensity decreases since competing reactions involving radicals occur in the system.

At the first stage, the effect of tungsten trioxide sol on chemiluminescence in the luminol-H_2O_2 system was studied. The WO_3 sol without a stabilizer increases the luminescence intensity by several times compared to the control therefore it exhibits prooxidant properties (Fig. 5A,B). When analyzing the PVP solution, a significant suppression of luminescence was observed (76±1% and 68±1% of the control with the addition of 25 and 50 μl of PVP, respectively) (Fig. 5B). The data obtained probably indicate the antioxidant properties of this stabilizer. Stabilization of the WO_3 sol with polyvinylpyrrolidone suppresses the prooxidant activity of tungsten oxide, the integrated luminescence intensities in the presence of WO_3–PVP and in the control sample are almost equal (Fig. 5B). Thus, the application of PVP as a stabilizer is desirable in cases where the prooxidant activity of WO_3 nanoparticles can have a negative effect.

The W–CC composite significantly suppresses luminescence in the H_2O_2/luminol system (Fig. 5C). The shape of the kinetic curve (chemiluminogram) characterizes the rate of reaction of the antioxidant with radicals and the duration of its action. In the case of W–CC, incomplete suppression of luminescence was observed, i.e., the W–CC composite is not a strong antioxidant. At the same time, W–CC is a long-acting antioxidant; it suppresses luminescence for a long time; no increase in luminescence intensity was observed on the chemiluminogram during the entire time of the experiment.

For a semi-quantitative evaluation of the antioxidant properties of the W–CC composite the antioxidant capacities of this composite, the PVP-stabilized WO_3 sol and the pharmaceutical antioxidant mexidol were measured. Antioxidant

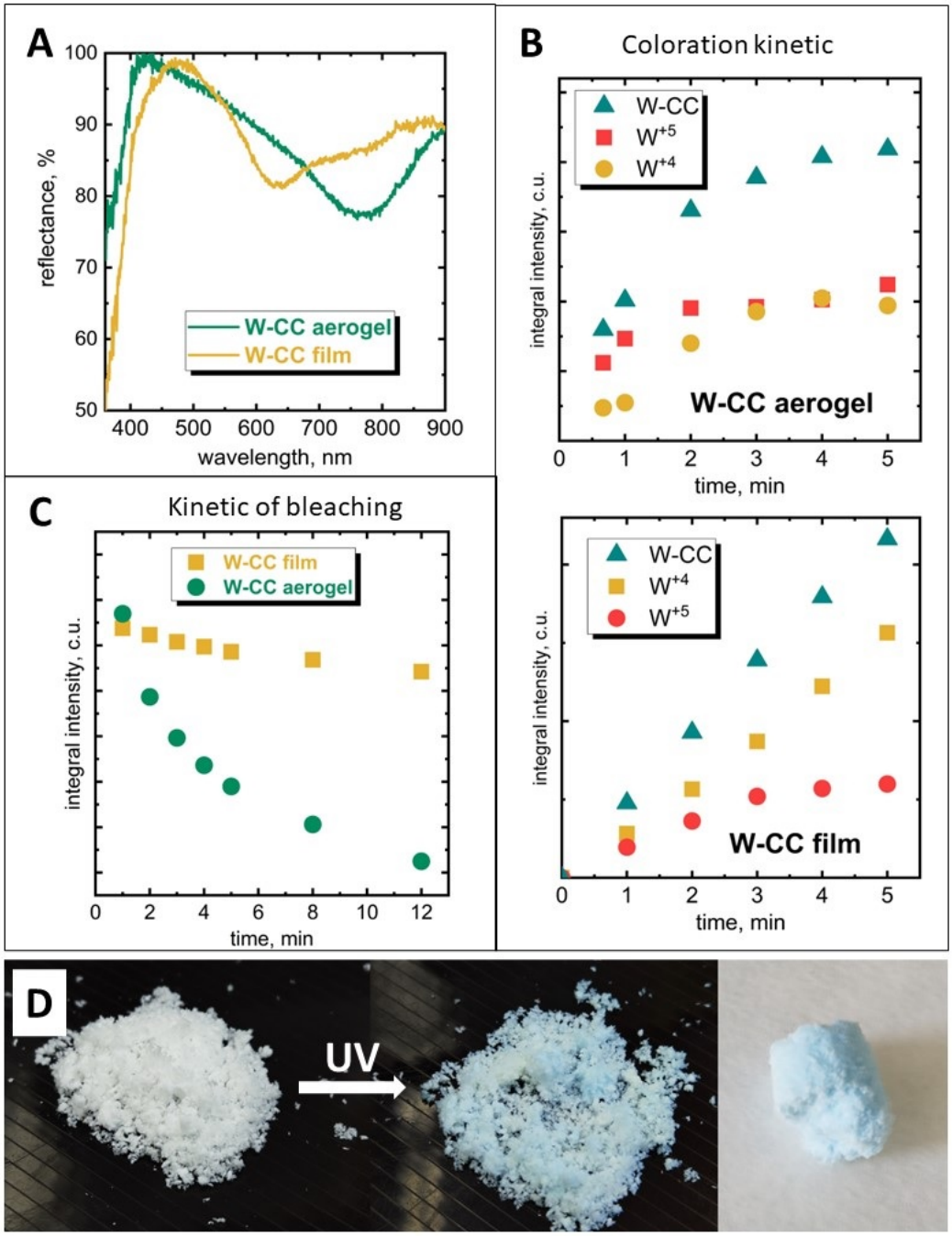

FIG. 4. UV-vis spectra of W–CC aerogel and film (A); coloration kinetics of the aerogel and the W–CC film (B): the integral intensities of absorption bands with peaks at 630 nm (W^{+4}) and 770 nm (W^{+5}), and total integral intensity (W–CC); bleaching kinetics of aerogel and W–CC film (C), total integral intensity of absorption bands at 630 and 770 nm; the image of W–CC aerogel before and after UV irradiation (D)

capacity (AC) is a numerical value proportional to the total amount of free radicals intercepted by a compound of a certain concentration. Antioxidant capacity is calculated as the difference between the areas under the kinetic curves (chemiluminograms) of the control sample and the investigated sample [37]. The antioxidant capacity of the test compound is usually expressed in AC units of one of the standard antioxidants. For this study a pharmaceutical antioxidant mexidol was chosen as the standard.

The antioxidant capacities of W–CC and WO_3 sol at low concentrations are somewhat higher than the antioxidant capacity of mexidol (Fig. 5D). The non-linear nature of the concentration dependence of W–CC antioxidant capacity is probably associated with a large number of various reaction centers on the surface of the composite and a complex mechanism for scavenging of hydroxyl radicals. Based on the experimental data, one can conclude that the antioxidant capacity of the W–CC composite at a concentration of 50 μM is 1.2 mexidol units, the antioxidant capacity of the WO_3 sol at a concentration of 50 μM is 1.5 mexidol units.

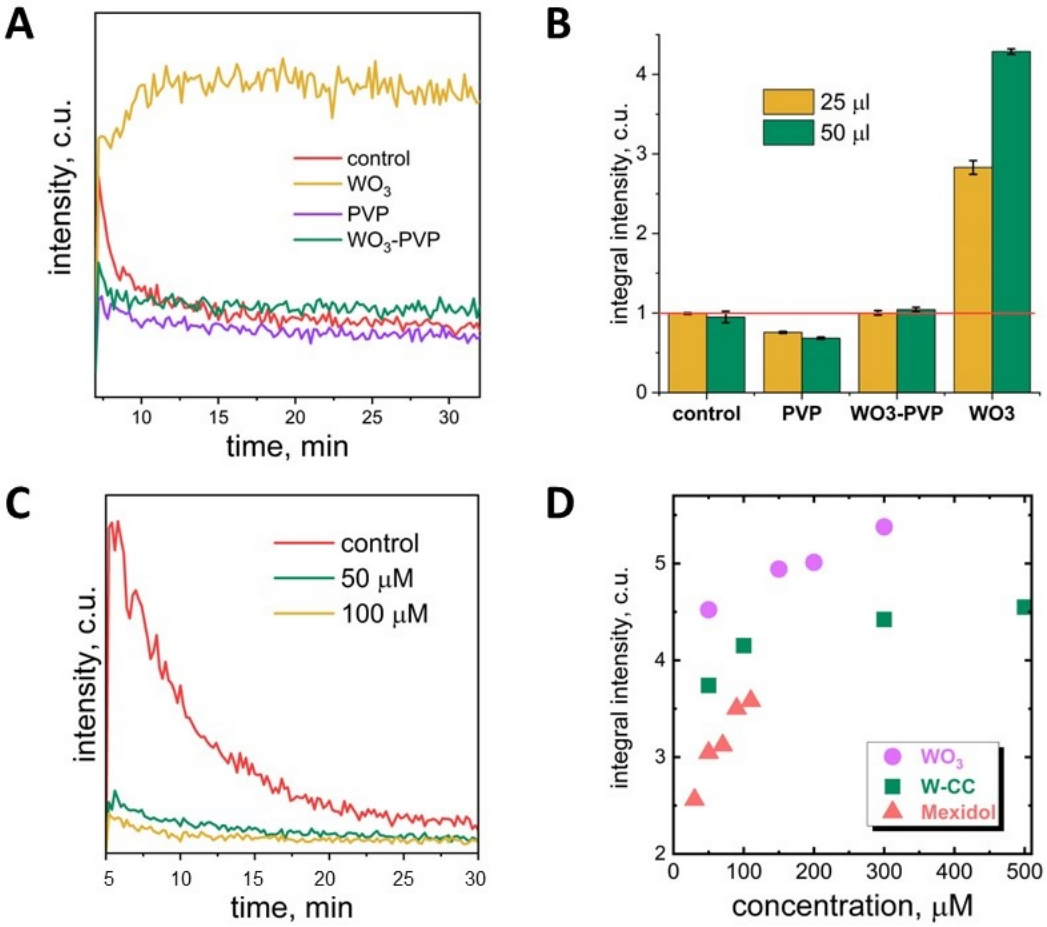

FIG. 5. Chemiluminogram of PVP, WO_3–PVP sol and uncoated WO_3 sol (A); histogram of the integral intensity of chemiluminescence curves of the control sample and samples of PVP, WO_3–PVP sol and uncoated WO_3 sol with concentrations of 25 and 50 μM (B); chemiluminogram of W–CC composite (C); antioxidant capacity of the WO_3–PVP sol, the W–CC composite and the standard antioxidant mexidol (D)

4. Summary

The photochromic hybrid aerogels and films based on TEMPO-oxidized cellulose and chitosan modified with ultrasmall (2 nm) tungsten trioxide nanoparticles were synthesized for the first time.

The synthesized hybrid aerogels and films have reversible photochromic properties. Under the action of UV radiation the materials turn blue within a few minutes as a result of the reduction of tungsten cations in WO_3 nanoparticles. In this case, in films W^{+6} is predominantly reduced to W^{+4}, while in the UV-Vis spectra of aerogels an intense W^{+5} absorption band was observed. Under the action of atmospheric oxygen in the dark the hybrid materials decolorize. The decoloration rate of aerogels is much higher than that of films due to the larger surface area (200 m^2/g) compared to films. The decoloration of the aerogel occurs within a few minutes, while the film decolorizes within five days. Due to

high decoloration rate, photochromic aerogel is a promising material for application in cyclic processes, for example, as a photocatalyst or a gas sensor.

The hybrid films and aerogels based on biopolymers modified with tungsten trioxide demonstrate antioxidant properties comparable to the pharmaceutical antioxidant drug mexidol. The antioxidant capacity of the W–CC composite is 1.2 units of mexidol at a concentration of 50 μM, the antioxidant capacity of the WO_3 sol is 1.5 units of mexidol at a concentration of 50 μM. Due to the use of polyanionic TEMPO-oxidized cellulose and polycationic chitosan as an organic matrix, hybrid films and aerogels retain their integrity when swollen in water. W–CC films absorb up to 8 g of water, while W–CC aerogels absorb up to 20 g of water per 1 g of material. Electrostatic binding of negatively charged WO_3 nanoparticles with a polycation (protonated chitosan) provides immobilization of inorganic particles in a biopolymer matrix. Thus, the synthesized hybrid materials have prospects for application as absorbent wound dressings with antioxidant properties.

References

[1] Budtova T. Cellulose II aerogels: a review. *Cellulose*, 2019, **26**(1), P. 81–121.

[2] Habibi Y., Lucia L.A., and Rojas O.J. Cellulose Nanocrystals: Chemistry, Self-Assembly, and Applications. *Chem. Rev.*, 2010, **110**, P. 3479–3500.

[3] Ganesan K. et al. Review on the production of polysaccharide aerogel particles. *Materials* (Basel)., 2018, **11**(11), P. 1–37.

[4] Abdul Khalil H.P., et al. A review on chitosan-cellulose blends and nanocellulose reinforced chitosan biocomposites: Properties and their applications. *Carbohydr. Polym.*, 2016, **150**, P. 216–226.

[5] William D., Connell O., Birkinshaw C., Francis T., and Dwyer O. Heavy metal adsorbents prepared from the modification of cellulose: A review. 2008, **99**, P. 6709–6724.

[6] Kaushik M. and Moores A. Review: Nanocelluloses as versatile supports for metal nanoparticles and their applications in catalysis. *Green Chem.*, 2016, **18**(3), P. 622–637.

[7] García-González C.A., Alnaief M., and Smirnova I. Polysaccharide-based aerogels—Promising biodegradable carriers for drug delivery systems. *Carbohydr. Polym.*, 2011, **86**(4), P. 1425–1438.

[8] Pircher N., et al. Preparation and Reinforcement of Dual-Porous Biocompatible Cellulose Scaffolds for Tissue Engineering. *Macromol. Mater. Eng.*, 2015, **300**(9), P. 911–924.

[9] Françon H., et al. Ambient-Dried, 3D-Printable and Electrically Conducting Cellulose Nanofiber Aerogels by Inclusion of Functional Polymers. *Adv. Funct. Mater.*, 2020, **30**(12), P. 1909383.

[10] Li Z., et al. Excellent reusable chitosan/cellulose aerogel as an oil and organic solvent absorbent. *Carbohydr. Polym.*, 2018, **191**, P. 183–190.

[11] Li V.C.F., Mulyadi A., Dunn C.K., Deng Y., and Qi H.J. Direct Ink Write 3D Printed Cellulose Nanofiber Aerogel Structures with Highly Deformable, Shape Recoverable, and Functionalizable Properties. *ACS Sustain. Chem. Eng.*, 2018, **6**(2), P. 2011–2022.

[12] Schestakow M., Muench F., Reimuth C., Ratke L., and Ensinger W. Electroless synthesis of cellulose-metal aerogel composites. *Appl. Phys. Lett.*, 2016, **108**(21), P. 213108, May.

[13] Li M. and Fu S. Photochromic holo-cellulose wood-based aerogel grafted azobenzene derivative by SI-ATRP. *Carbohydr. Polym.*, 2021, **259**, P. 117736.

[14] Yamazaki S., Ishida H., Shimizu D., and Adachi K. Photochromic Properties of Tungsten Oxide/Methylcellulose Composite Film Containing Dispersing Agents. *ACS Appl. Mater. Interfaces*, 2015, **7**(47), P. 26326–26332.

[15] Adachi K., et al. Kinetic characteristics of enhanced photochromism in tungsten oxide nanocolloid adsorbed on cellulose substrates, studied by total internal reflection Raman spectroscopy. *RSC Adv.*, 2012, **2**(5), P. 2128–2136.

[16] Zhang Q., Wang R., Lu Y., Wu Y., Yuan J., and Liu J. Highly Efficient Photochromic Tungsten Oxide@PNIPAM Composite Spheres with a Fast Response. *ACS Appl. Mater. Interfaces*, 2021, **13**(3), P. 4220–4229.

[17] Dong C., Zhao R., Yao L., Ran Y., Zhang X., and Wang Y. A review on WO_3 based gas sensors: Morphology control and enhanced sensing properties. *J. Alloys Compd.*, 2020, **820**, P. 153194.

[18] Guo X.Z., Kang Y.F., Yang T.L., and Wang S.R. Low-temperature NO_2 sensors based on polythiophene/WO_3 organic-inorganic hybrids. *Trans. Nonferrous Met. Soc.* China (English Ed.), 2012, **22**(2) P. 380–385.

[19] Yu H., et al. Colloidal synthesis of tungsten oxide quantum dots for sensitive and selective H_2S gas detection. *Sensors Actuators, B Chem.*, 2017, **248**, P. 1029–1036.

[20] El Fawal G.F., Abu-Serie M.M., Hassan M.A., and Elnouby M.S. Hydroxyethyl cellulose hydrogel for wound dressing: Fabrication, characterization and in vitro evaluation. *Int. J. Biol. Macromol.*, 2018, **111**, P. 649–659.

[21] Popov A.L., et al. Photo-induced toxicity of tungsten oxide photochromic nanoparticles. *J. Photochem. Photobiol. B Biol.*, 2018, **178**, P. 395–403.

[22] D'Autréaux B. and Toledano M.B. ROS as signalling molecules: mechanisms that generate specificity in ROS homeostasis. *Nat. Rev. Mol. Cell Biol.*, 2007, **8**(10), P. 813–824.

[23] Ciccarese F., Raimondi V., Sharova E., Silic-Benussi M., and Ciminale V. Nanoparticles as Tools to Target Redox Homeostasis in Cancer Cells. *Antioxidants*, 2020, **9**(3), P. 211.

[24] Kwon S., Ko H., You D.G., Kataoka K., and Park J.H. Nanomedicines for Reactive Oxygen Species Mediated Approach: An Emerging Paradigm for Cancer Treatment. *Acc. Chem. Res.*, 2019, **52**(7), P. 1771–1782.

[25] Di Marzo N., Chisci E., and Giovannoni R. The Role of Hydrogen Peroxide in Redox-Dependent Signaling: Homeostatic and Pathological Responses in Mammalian Cells. *Cells*, 2018, **7**(10), P. 156.

[26] Costa T.J., et al. The homeostatic role of hydrogen peroxide, superoxide anion and nitric oxide in the vasculature. *Free Radic. Biol. Med.*, 2021, **162**, P. 615–635.

[27] Evdokimova O.L., et al. Highly reversible photochromism in composite WO_3/nanocellulose films. *Cellulose*, 2019, **26**, P. 9095–9105.

[28] Sozarukova M.M., Proskurnina E.V., and Ivanov V.K. Prooxidant potential of ceo2 nanoparticles towards hydrogen peroxide. *Nanosyst. Physics, Chem. Math.*, 2021, **12**(3), P. 283–290.

[29] Fayad A.M., Ouis M.A., El Batal F.H., and El Batal H.A. Shielding Behavior of Gamma-Irradiated MoO_3 or WO_3-Doped Lead Phosphate Glasses Assessed by Optical and FT Infrared Absorption Spectral Measurements. *Silicon*, 2018, **10**, P. 1873–1879.

[30] Loo A.E.K., et al. Effects of Hydrogen Peroxide on Wound Healing in Mice in Relation to Oxidative Damage. *PLoS One*, 2012, **7**(11), P. e49215.

[31] Stone J.R. and Yang S. Hydrogen Peroxide: A Signaling Messenger. *Antioxid. Redox Signal.*, 2006, **8**(3–4), 243–270.

[32] Di Marzo N., Chisci E., and Giovannoni R. The Role of Hydrogen Peroxide in Redox-Dependent Signaling: Homeostatic and Pathological Responses in Mammalian Cells. *Cells*, 2018, **7**(10), P. 156.

[33] Lismont C., Revenco I., and Fransen M. Peroxisomal Hydrogen Peroxide Metabolism and Signaling in Health and Disease. *International Journal of Molecular Sciences*, 2019, **20**(15), P. 3673.

[34] Pirmohamed T., et al. Nanoceria exhibit redox state-dependent catalase mimetic activity. *Chem. Commun.*, 2010, **46**(16), P. 2736–2738.

[35] Hu M., Korschelt K., Daniel P., Landfester K., Tremel W., and Bannwarth M.B. Fibrous Nanozyme Dressings with Catalase-Like Activity for H_2O_2 Reduction To Promote Wound Healing. *ACS Appl. Mater. Interfaces*, 2017, **9**(43), P. 38024–38031.

[36] Wei H. and Wang E. Nanomaterials with enzyme-like characteristics (nanozymes): next-generation artificial enzymes. *Chem. Soc. Rev.*, 2013, **42**(14), P. 6060–6093.

[37] Sozarukova M.M., Shestakova M.A., Teplonogova M.A., Izmailov D.Y., Proskurnina E.V., and Ivanov V.K. Quantification of Free Radical Scavenging Properties and SOD-Like Activity of Cerium Dioxide Nanoparticles in Biochemical Models. *Russ. J. Inorg. Chem.*, 2020, **65**(4), P. 597–605.

Submitted 5 May 2022; accepted 15 June 2022

Information about the authors:

Svetlana V. Kameneva – Kurnakov Institute of General and Inorganic Chemistry of the Russian Academy of Sciences, Leninsky Prospekt, 31, Moscow, 119991, Russia; kamenevasvetlanav@gmail.com

Matvei A. Popkov – Kurnakov Institute of General and Inorganic Chemistry of the Russian Academy of Sciences, Leninsky Prospekt, 31, Moscow, 119991, Russia; Lomonosov Moscow State University, Leninskye gory, 1, Moscow, 119991, Russia; popkovma2001@mail.ru

Ilya V. Tronev – Kurnakov Institute of General and Inorganic Chemistry of the Russian Academy of Sciences, Leninsky Prospekt, 31, Moscow, 119991, Russia; HSE University, Myasnitskaya, 20, Moscow, 101000, Russia; ivtronev@edu.hse.ru

Sergey Yu. Kottsov – Kurnakov Institute of General and Inorganic Chemistry of the Russian Academy of Sciences, Leninsky Prospekt, 31, Moscow, 119991, Russia; Lomonosov Moscow State University, Leninskye gory, 1, Moscow, 119991, Russia; sergey12-17@yandex.ru

Madina M. Sozarukova – Kurnakov Institute of General and Inorganic Chemistry of the Russian Academy of Sciences, Leninsky Prospekt, 31, Moscow, 119991, Russia; s_madinam@bk.ru

Vladimir K. Ivanov – Kurnakov Institute of General and Inorganic Chemistry of the Russian Academy of Sciences, Leninsky Prospekt, 31, Moscow, 119991, Russia; van@igic.ras.ru

Conflict of interest: the authors declare no conflict of interest.